Mycobacteria-induced granuloma necrosis depends on IRF-1

Sahar Aly [a, #], Jörg Mages [b, #], Norbert Reiling [a], Ulrich Kalinke [c], Thomas Decker [d], Roland Lang [b, †, ‡], Stefan Ehlers [a, e, †, *]

[a] Molecular Infection Biology, Research Center Borstel, Borstel, Germany,
[b] Medical Microbiology, Immunology and Hygiene, Technical University of Munich, München, Germany
[c] Immunology, Paul-Ehrlich-Institut, Langen, Germany
[d] Microbiology and Immunobiology, University of Vienna, Wien, Austria
[e] Molecular Inflammation Medicine, Christian-Albrechts – University Kiel, Kiel, Germany

Received: March 19, 2008; Accepted: August 7, 2008

Abstract

In a mouse model of mycobacteria-induced immunopathology, wild-type C57BL/6 (WT), IL-18-knockout (KO) and IFN-αβ receptor-KO mice developed circumscript, centrally necrotizing granulomatous lesions in response to aerosol infection with *M. avium*, whereas mice deficient in the IFN-γ receptor, STAT-1 or IRF-1 did not exhibit granuloma necrosis. Comparative, microarray-based gene expression analysis in the lungs of infected WT and IRF-1-KO mice identified a set of genes whose differential regulation was closely associated with granuloma necrosis, among them cathepsin K, cystatin F and matrix metalloprotease 10. Further microarray-based comparison of gene expression in the lungs of infected WT, IFN-γ-KO and IRF-1-KO mice revealed four distinct clusters of genes with variable dependence on the presence of IFN-γ, IRF-1 or both. In particular, IRF-1 appeared to be directly involved in the differentiation of a type I immune response to mycobacterial infection. In summary, IRF-1, rather than being a mere transcription factor downstream of IFN-γ, may be a master regulator of mycobacteria-induced immunopathology.

Keywords: inflammation • tuberculosis • granuloma • necrosis • immunopathology • interferon • microarray

Introduction

Granuloma necrosis is the pathological hallmark of human pulmonary tuberculosis (TB) [1]. Granuloma necrosis not only causes irreversible tissue damage and impairment of lung function; it is also the prerequisite for the eruption of granuloma contents into the airways and the dissemination of the causative mycobacterium *via* aerosol into the environment [2]. Modulating the immunopathology of TB by preventing or mitigating granuloma necrosis therefore represents an attractive means by which adjuvant immunotherapy might favourably alter the course of disease progression.

The molecular mechanisms of granuloma necrosis remain largely unknown because the only genetically and immunologically tractable animal model of TB, the laboratory mouse, does not mimic the disease pathology present in human beings [3]. Rather, aerosol infection with *M. tuberculosis* causes progressive interstitial lung fibrosis, but does not lead to circumscript centrally necrotizing lesions in immunocompetent mice [3]. However, using a particular strain of a related mycobacterial species, *M. avium* TMC724, a mouse model of mycobacteria-induced immunopathology was developed in which central granuloma necrosis, similar to human TB lesions, does occur and is causally related to the presence of T cells and IFN-γ [4, 5]. Recently, a case was made for the involvement of angiostatic chemokines and the development of hypoxia in the necrotizing process of chronic granulomatous lesions [6].

The signalling events downstream of IFN-γ are the subject of this communication. By using mice singly deficient in individual elements of the IFN-signalling pathway, we identified the IFN-γ/STAT1/IRF-1 axis as the master regulator of granuloma necrosis. Furthermore, comparative microarray-based gene expression analysis in IFN-γ-deficient, IRF-1-deficient and wild-type (WT) mice defined a number of genes whose regulation was closely associated with mycobacteria-induced immunopathology and which may now be used to test the hypothesis that tissue-damaging events may be molecularly distinct from antibacterially protective mechanisms.

[#] S.A. and J.M. contributed equally as first authors.
[†] R.L. and S.E. contributed equally as senior authors.
[‡] Current address: Institute of Clinical Microbiology, Immunology and Hygiene, University Erlangen-Nürnberg, Wasserturmstr. 3-5, 91054, Erlangen, Germany.
*Correspondence to: Prof. Dr. S. EHLERS,
Research Center Borstel, Parkallee 22, D-23845 Borstel, Germany.
Tel.: +49-4537-188481
Fax: +49-4537-188406
E-mail: sehlers@fz-borstel.de; roland.lang@uk.erlangen.de

doi: 10.1111/j.1582-4934.2008.00470.x

Materials and methods

Mice

Selectively gene-deficient (knockout, KO) mice backcrossed for at least 10 generations to a C57BL/6 background were used together with age- and sex-matched C57BL/6 (WT) mice. IFN-γ receptor-KO, IRF-1-KO and the corresponding WT mice were purchased from The Jackson Laboratory, Bar Harbor, ME, USA. IL-18-KO mice were used with permission from S. Akira. IFN-α/β receptor-KO mice were bred at the Paul-Ehrlich-Institute, Langen, Germany. STAT-1-KO mice were bred at the Department of Microbiology and Immunobiology, Vienna, Austria. Mice were free of viral, bacterial and parasitic mouse pathogens, as certified by routine screens at the breeding centres according to Federation of European Laboratory Animal Science Associations (FELASA) regulations.

Infection of mice

M. avium TMC724 was prepared and used for infection protocols as described [5, 7]. In a respiratory infection model, mice were exposed to an aerosol containing *M. avium* TMC724 using an aerosol inhalation device (Glas-Col, Terre-Haute, IN, USA) calibrated to deposit 10^5 colony forming units (CFU) *M. avium* in the lungs of mice. Groups of four to five mice were anaesthetized by a narcotic overdose and killed at indicated time-points. The bacterial load was determined by serial dilutions of organ homogenates on 7H10 agar plates supplemented with 10% bovine serum (Biowest, Nuaillé, France). Mice were killed when their weight loss exceeded 25% compared to that of non-infected, age- and sex-matched littermates.

Histology and immunohistology

Four per cent formalin-fixed, paraffin-embedded organs were cut, mounted on glass slides and stained with standard haematoxylin and eosin. For the detection of cathepsin K, antigen retrieval was carried out on deparaffinized tissues with pronase (Fisher Scientific, Schwerte, Germany) for 40 min. at 40°C. Reduction of endogenous peroxidase activity was performed with 0.03% hydrogen peroxide for 5 min. at room temperature. The cross-reactive mouse anti-human cathepsin K monoclonal antibody (Chemicon, Hampshire, United Kingdom), pre-labelled for 15 min. with a biotinylation reagent (Dako, Hamburg, Germany), was applied for 15 min. The reaction was visualized using streptavidin conjugated to horseradish peroxidase followed by its substrate 3,3′-diaminobenzidine (Dako). Tissue sections were counterstained with Mayer's haematoxylin and mounted.

ELISA

Levels of IFN-γ (BD Pharmingen, San Diego, CA, USA) protein in the lung homogenates were measured with commercial OptEIA Cytokine ELISA kits, as described [8]. Lungs were harvested 14 and 20 weeks after infection with *M. avium,* homogenized in 10 mM phosphate-buffered saline containing a proteinase inhibitor mixture (Roche Diagnostics Applied Science, Mannheim, Germany) and stored at –70°C. Absorption was measured at 450 nm against a 620-nm reference wavelength by an ELISA Reader. The cytokine concentration was evaluated using Magellan software (TECAN) and calculated for total organ weight.

Affymetrix gene expression microarrays

Total cellular RNA from lung tissue was prepared as described [9, 10], but the phenol/chloroform extraction was performed using TriFast FL (PeqLab, Erlangen, Germany). Total RNA (1 μg) was labelled and hybridized to Affymetrix mouse MOE430A 2.0 GeneChips according to the manufacturer's recommendations. For each condition (WT and IRF-1-KO, infected or uninfected) three biological replicates were used. Affymetrix CEL files were processed for global normalization and generation of expression values using the robust multi-array average algorithm (RMA) in the R affy package (http://www.r-project.org).

To analyse the IRF-1-dependent effects in infection, a two-way ANOVA was performed, using the ANOVA function in R. The resulting *P*-values were corrected for multiple testing using the algorithm proposed by Benjamini and Hochberg [11], implemented in the R multitest package (output: *q*-values). Stringent criteria were used to define genes as significantly regulated upon infection: *q*-values below 0.01 and a fold-change (ratio of the average expression values of infected compared with the respective uninfected samples) filter above 2 or below 0.5. Significantly regulated genes were clustered according to similar regulation patterns using the program Genesis (release 1.6.0) [12] or by *k*-means clustering in R.

For a comparative analysis of IRF-1- and IFN-γ-dependent gene expression, a previously described dataset from an independent *M. avium* infection experiment in WT and IFN-γ-KO mice [6] was re-analysed together with the microarray data from WT and IRF-1-KO lungs described above. Cel files from both experiments were normalized together using RMA [13]. Regulated genes were identified by a combination of statistical testing (limma F-test $P < 0.0001$) and absolute and relative changes in expression across all conditions (max-min > 80, max/min > 3). The resulting 2278 probe sets were then used for a *k*-means cluster analysis.

All microarray data have been deposited in the Gene Expression Omnibus (accession number GSE 11809).

RT-PCR

One microgram of total RNA was reverse-transcribed with an oligo(dT)12–18 primer (Amersham Biosciences, Uppsala, Sweden) in the presence of Moloney murine leukaemia virus reverse transcriptase (Fermentas, Ontario, Canada). The resulting cDNA was amplified on a Light Cycler (Roche Diagnostics Corporation) using the proprietary Light-Cycler-DNA Master SYBR Green I kit (Roche Diagnostics Corporation) and the following primer sets: HPRT – sense, 5′-GCC AGT AAA ATT AGC AGG TGT TCT, antisense, 3′-AGG CTC ATA GTG CAA ATC AAA AGT C; MMP-10 – sense, 5′-GAG TCT GGC TCA TGC CTA CC, antisense, 3′-CAG GAA TAA GTT GGT CCC TGA; Ctsk – sense, 5′-CGA AAA GAG CCT AGC GAA CA, antisense, 3′-TGG GTA GCA GCA GAA ACT TG; Cst7 – sense, 5′- GGA GTC CCA TGT CAG CAA AG, antisense, 3′- GGT CTT CCT GCA TGT AGT TCG; Tspan31 – sense, 5′-GCG CTC TCA ACG TGG TTT AT, antisense, 3′-TCC TCC AAT GAT GTG AAT GC (HPRT: hypoxanthine phosphoribosyltransferase as housekeeping gene, MMP-10: matrix metalloproteinase 10, Ctsk: cathepsin K, Cst7: cystatin F, Tspan31: tetraspanin 31).

After amplification, melting curve analysis was performed to exclude the presence of confounding primer dimers. Semi-quantitative comparisons of amplified products were made based on the crossing points obtained for each sample compared with a serially diluted, arbitrarily selected standard cDNA run in parallel. In this way, arbitrary units could be assigned to mRNA levels present in each sample. The ratio of arbitrary

units of the gene of interest and arbitrary units of the housekeeping gene HPRT was multiplied by 100 for each sample.

Data shown in Fig. 8 were generated using cDNA reverse transcribed from 1 μg of lung RNA with a combined oligo dT(12–18)/random hexamer primed first strand synthesis. For qRT-PCR, the Roche Universal Probe Library system was used to select specific primers and probes. Sequences are available upon request from the authors. PCR was carried out for 45 cycles. Data were processed according to the ΔΔCT method, using HPRT as housekeeping gene for normalization and the mock treated IRF-$1^{+/+}$ lung RNA as a calibrator for calculation of fold changes.

Determination of MMP activity in infected tissues

MMP activity in lung homogenates of infected mice at the indicated time-points was analysed using the fluorogenic peptide Mca-PLGL-Dpa-AR-NH2 (R&D Systems, Wiesbaden, Germany), a substrate for MMP-1 (collagenase 1), MMP-2 (gelatinase A), MMP-7 (matrilysin), MMP-8 (collagenase 2), MMP-9 (gelatinase B), MMP-12 (macrophage elastase), MMP-13 (collagenase 3), MMP-14 (MT1-MMP), MMP-15 (MT2-MMP) and MMP-16 (MT3-MMP) [14]. A second peptide Mca-RPKPVE-Nval-WRK (Dnp)-NH2, (R&D Systems) was used to monitor the activity of MMP-3 (stromelysin 1), MMP-10 (stromelysin 2), trypsin, HGF activator and factor Xa 2 [15]. Assays were performed according to the manufacturer's instructions. In brief, aliquots of the homogenate were centrifuged at 300 × *g* for 10 min. Equal amounts of the supernatants were incubated at RT for 30 min. and measured using a fluorescence microplate reader (Genios, Tecan, Crailsheim, Germany) with excitation at 320 nm and emission at 405 nm. The measured relative light units (RLU) were correlated to milligrams protein in the lung homogenate and depicted as MMP activity [RLU/mg].

Statistics

Means, S.D.s and statistics for quantifiable data, such as CFU counts were calculated using Microsoft Office Excel 2003 for Windows and GraphPad Prism version 4.00 for Windows (GraphPad Software, San Diego, CA, USA; www.graphpad.com). Significance of the difference at a given time-point was analysed using one-way ANOVA, setting the confidence level at 99%. If not specifically indicated by an asterisk, the *P*-value is above 0.01 and there is no significant difference at a confidence level of 99%.

Results

IFN-γ signalling *via* STAT-1 and IRF-1 is crucial for the development of granuloma necrosis

C57BL/6 and STAT-1-KO mice were infected with 10^5 CFU *M. avium* TMC724 by aerosol. Sixteen weeks post-infection tissue sections of the lung were stained with haematoxylin and eosin to determine the degree of granuloma formation and necrosis. Central necrosis was never observed in inflammatory infiltrates of STAT-1-KO mice (Fig. 1B), but excessive granulocyte influx was evident, with predominating aggregates of neutrophils interconnected by 'avenues' of granulocytes. In contrast, a well-defined necrotic core, surrounded by a granulocytic rim and a belt of epithelioid macrophages, was apparent in the WT mice already at 14 weeks after infection (Fig. 1A), confirming that intact IFN-γ signalling *via* STAT-1 is essential for the development of granuloma necrosis in this mycobacterial infection model [4].

STAT-1 transduces signals from both the IFN type I as well as the IFN type II receptor. To determine the critical inducer receptor of STAT-1-mediated granuloma necrosis, IFN-α/β-R-KO, IFN-γ-R-KO and C57BL/6 mice were infected with 10^5 CFU *M. avium* TMC724. In addition, IL-18-KO mice were analysed in this model, because both IL-12 and IL-18 have been described to induce IFN-γ, thereby initiating a protective Th1-immune response [16, 17]. Mice deficient for IL-12 (p40, or both, p35 and p40 chains), however, are already known not to develop granuloma necrosis in this model [4]. IFN-γ levels in infected lungs of IL-18-KO mice were significantly reduced to less than one-third of that present in WT mice at 14 weeks after infection (2412 *versus* 8020 pg/g lung), while 20 weeks after infection IFN-γ levels were similarly low in both IL-18-KO and WT mice (518 *versus* 667 pg/g lung, respectively).

Eighteen to 24 weeks post-infection circumscript, central granuloma necrosis was evident in IFN-α/β-R-KO and IL-18-KO mice as well as in WT mice (Fig. 1A, C and D). In all three mouse strains, a central mass composed of acellular debris was demarcated by a rim of densely accumulating granulocytes surrounded by prominent layers of epithelioid macrophages and fibroblasts. On the other hand, IFN-γ-R-KO mice did not develop granuloma necrosis (Fig. 1E), but showed signs of widespread, diffuse tissue damage without a clear demarcation of caseating foci, similar to IFN-γ-KO mice [5]. IFN-γ- and STAT1-mediated signalling proceeds in part *via* the transcriptional activator, IRF-1. Indeed, IRF-1-KO mice infected with *M. avium* TMC724, were completely devoid of central granuloma necrosis and instead displayed diffuse and mixed cellular infiltrates (Fig. 1F).

Thus, IFN type I signalling is not necessary for the development of central granuloma necrotization in the lungs of mice infected with *M. avium* TMC724, whereas IFN-γ, IFN-γ-R, STAT-1 and IRF-1 play a crucial role.

IFN-γ signalling *via* STAT-1 is crucial for retarding *M. avium* growth and premature death, whereas IRF-1 dependent signalling is less critical

The bacterial load in the lungs of IFN-αβ receptor-KO mice and IL-18-KO mice (not shown) was almost identical to that observed in WT mice (between 10^{10} and 10^{11} CFU/lung at 18 weeks after infection), whereas IFN-γ-R-KO, STAT-1-KO and IRF-1-KO mice infected with *M. avium* had a higher bacterial burden (between 10^{11} and 10^{12} CFU/lung) than C57BL/6 mice at least at one time-point following infection (Fig. 2). *M. avium*-infected C57BL/6 mice survived significantly longer than IFN-γ-KO and STAT-1-KO

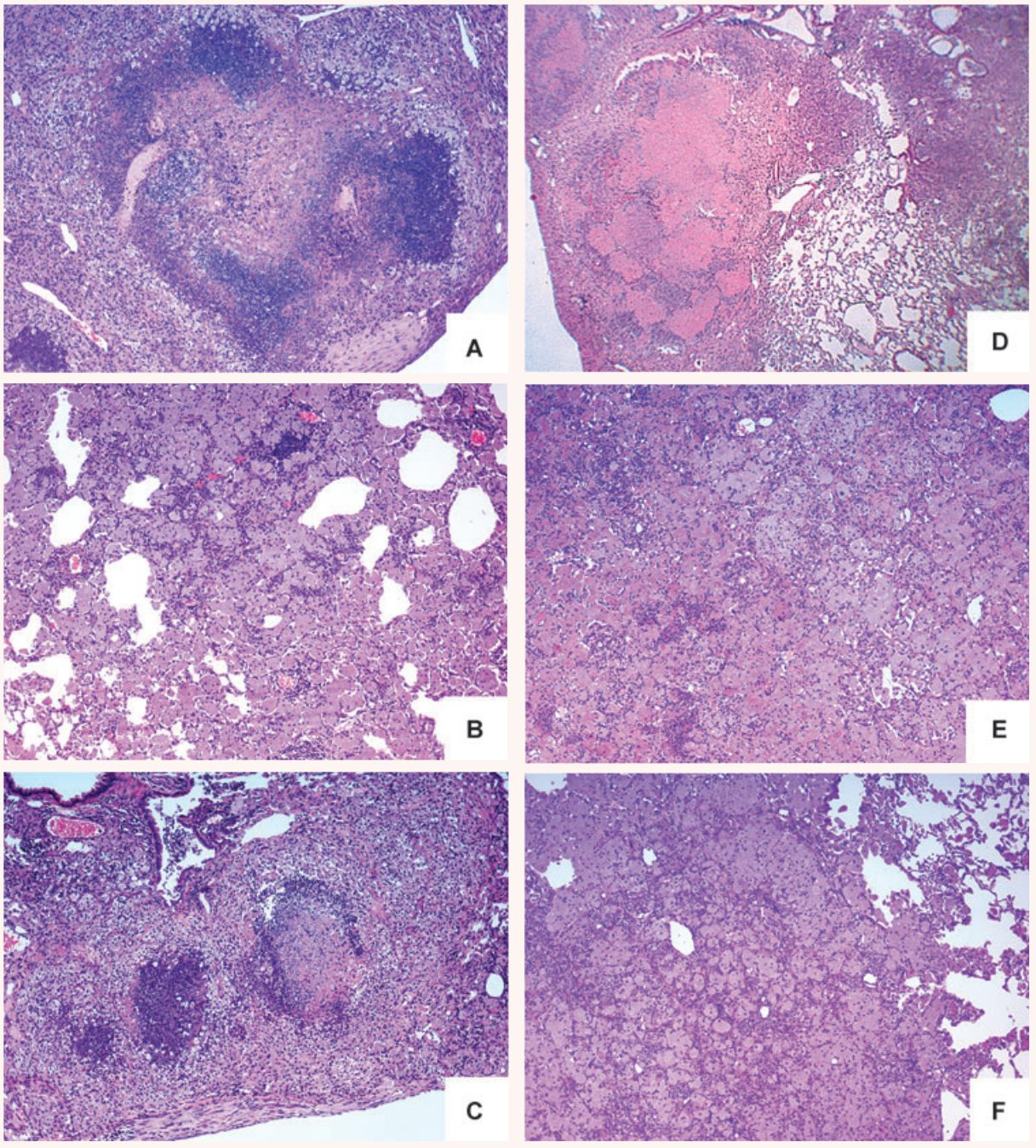

Fig. 1 Granuloma morphology in interferon pathway deficient mice. Histopathologies shown are from C57BL/6 (**A**), STAT-1-KO (**B**), IFN-αβ-R-KO (**C**), IL-18-KO (**D**), IFN-γ-R-KO (**E**) and IRF-1-KO (**F**) mice infected with *M. avium* (TMC724, 10^5 CFU/mouse) by aerosol. *M. avium*-infected lungs were removed 16 weeks after infection from WT, STAT-1-KO and IFN-γ-R-KO mice and after 20–24 weeks after infection in IFN-αβ-R-Ko, IL-18-KO and IRF-1-KO mice. Lung sections were stained with haematoxylin and eosin (original magnification ×10). Micrographs are representative of four mice examined.

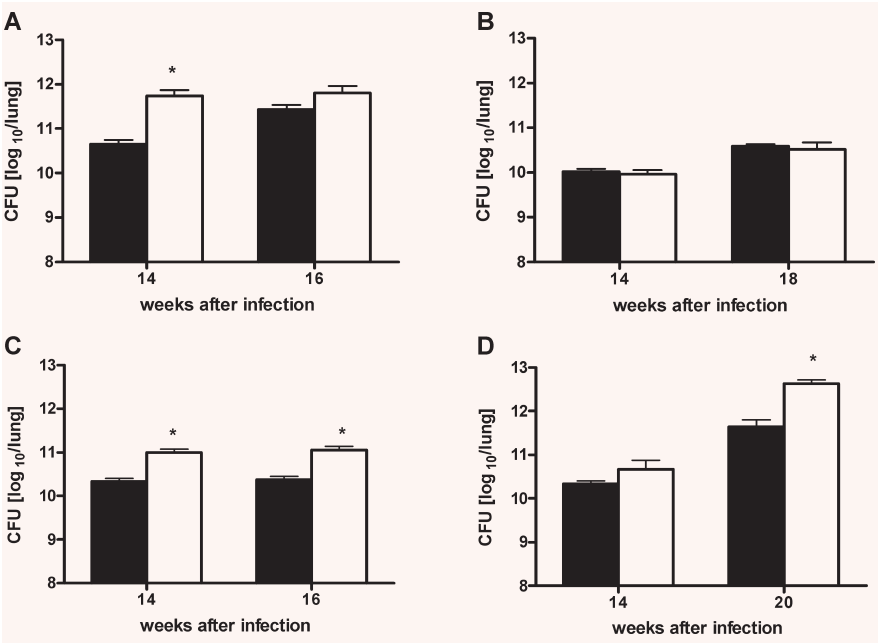

Fig. 2 Bacterial loads in interferon pathway deficient mice. Mice were infected with *M. avium* by aerosol in separate experiments, each with its own WT control strain, and killed at indicated timepoints to determine mycobacterial loads in the lung. (**A**) C57BL/6 (black bars), STAT-1-KO (white bars); (**B**) C57BL/6 (black bars) and IFN-αβ-R-KO (white bars); (**C**) C57BL/6 (black bars), IFN-γ-R-KO (white bars) and (**D**) C57BL/6 (black bars) and IRF-1-KO (white bars). Data represent the means of four mice ± S.D. $*P < 0.01$ at a confidence level of 99%.

Table 1 Mean survival times of various *M. avium*-infected gene-deficient mouse strains

Experimental mouse strains	Wild-type (WT) (days)	Knockout (KO) (days)	Statistics (*P*-value)
WT *versus* IFN-γ-KO	138	93	<0.05
WT *versus* IFN-γ-R-KO	150	105	ND
WT *versus* IFN-αβ-R-KO	145	157	>0.05
WT *versus* IL-18-KO	165	150	>0.05
WT *versus* STAT-1-KO	137	96	<0.05
T *versus* IRF-1-KO	128	155	ND

WT and indicated KO mouse strains were infected by aerosol with *M. avium* TMC724 in separate experiments, each with its own WT control. Mice were killed when their weight loss exceeded 25% of uninfected controls. Indicated is the mean time to death for each mouse strain in days after infection. ND: statistics not performed due to low number of mice in experiment.

mice whereas there was no significant difference in the survival rate of *M. avium*-infected C57BL/6, IFN-αβ-R-KO and IRF-1-KO mice (Table 1).

Therefore, STAT-1 signalling is involved in tissue pathology, *M. avium* growth control and survival, whereas the IRF-1-dependent signalling is important for granuloma necrosis but less so for the control of bacterial replication and overall survival.

Comparative evaluation of gene expression in the lungs of infected WT and IRF-1-KO mice reveals a set of genes associated with granuloma necrosis

To obtain an unbiased view of the impact of IRF-1 deficiency on the transcriptional changes in the lung following infection with *M. avium*, gene expression profiling using Affymetrix GeneChips was performed on lung tissue RNA harvested 14 weeks after infection. Using stringent statistical and fold-change filters, we found 3022 genes significantly regulated in WT mice and 1489 in IRF-1-KO mice in the dataset, with a significant interaction of the covariates 'infection' and 'genotype' in 528 genes. Hierarchical cluster analysis of this group of genes demonstrates that the majority are strongly up- or down-regulated in infected WT lungs but not in IRF-1-KO (Fig. 3A, clusters B and D, respectively). A smaller group shows the reverse pattern of expression, with a strong increase in IRF-1-KO lungs (cluster E). A comprehensive list of genes regulated more than fivefold is provided in Table S1. Interestingly, as previously described [18], some chemokines stood out, in particular the CXC ligands 5, 10 and 11 as well as the CC ligands 5 and 19, in WT mice although they were expressed at significantly lower levels in the lungs of infected IRF-1-KO mice.

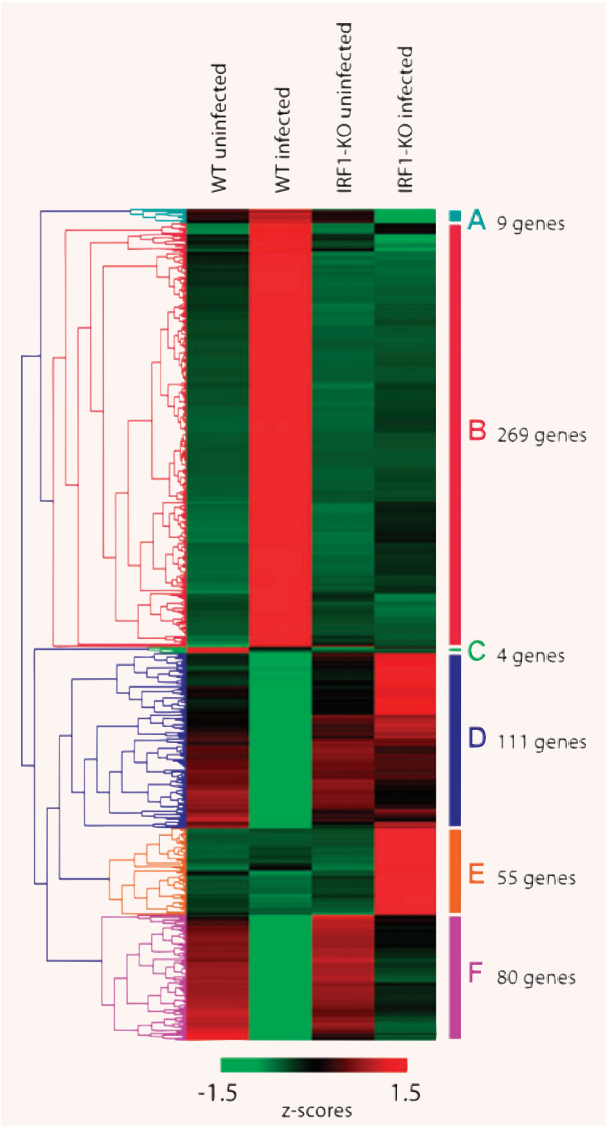

Fig. 3 Differential gene expression in the lungs of WT *versus* IRF-1-KO mice. WT and IRF-1-KO mice were infected by aerosol with *M. avium* (TMC724, 10^5 CFU/mouse). Total RNA was prepared from the right lungs harvested 14 weeks after infection as well as from the right lungs of uninfected mice, and processed for gene expression analysis *via* microarrays. This is a graphic representation of a cluster analysis including 528 genes regulated more than twofold between WT and IRF-1 KO lungs infected with *M. avium* and significantly in a two-way ANOVA with the covariates infection status and genotype (q-value < 0.01). Expression data from three animals per condition were z-score normalized and analysed by hierarchical clustering. Each row in the heat map represents one probe set, the columns stand for the conditions tested. A red square indicates higher expression, a green square indicates lower expression relative to a row-wise mean (black). The different groups (**A**)–(**F**) comprise genes regulated in a similar manner.

To derive more specific information about the biological process and pathways affected by IRF-1 deficiency in *M. avium*-infected mice, we mined the different clusters for enrichment of functional annotation terms in the gene ontology (GO) category biological process [19]. A selection of significantly enriched terms together with handpicked example genes is depicted in Table 2. The IRF-1-dependent cluster B was highly enriched for 'defence response' and 'inflammatory response' genes. Furthermore, cluster B genes are functionally linked to antigen processing and presentation, as well as B- and T-cell activation. Of particular interest in relation to the mechanisms of granuloma necrosis, genes linked to cell death and apoptosis were also significantly overrepresented in this cluster. In contrast, for the smaller group of genes overexpressed in IRF-1-KO infected lungs, significant enrichment was only found for genes involved in chitin/carbohydrate catabolism.

Verification of candidate genes by RT-PCR, immunohistology and activity assays

Within the subset of genes differentially regulated more than five-fold in WT compared to IRF-1-KO mice (Table S1), a number of proteolysis-associated genes were apparent, in particular those for MMP-10, cathepsin K and cystatin F. Although cathepsin K was up-regulated in KO mice, its inhibitor cystatin F as well as MMP-10 appeared up-regulated to a much higher extent in WT than in KO mice.

In order to confirm these microarray data, mRNA quantitation by Light Cycler RT-PCR was performed to compare MMP-10, cathepsin K and cystatin F mRNA levels (as well as tetraspanin 31 as an unregulated control mRNA) in WT *versus* IRF-1-KO mice (Fig. 4). MMP-10 and cystatin F mRNA levels were approximately 70-fold lower in IRF-1-KO compared to WT mice, and cathepsin K mRNA levels were approximately 50-fold higher in IRF-1-KO compared to WT mice, essentially corroborating microarray results.

Further, immunohistochemistry in the lung tissue of WT and IRF-1-KO mice (Fig. 5) revealed that cathepsin K could not be detected in granulomatous infiltrations of WT mice, whereas IRF-1 KO mice harboured many cathepsin-K-expressing cells in infected lungs, particularly foamy macrophages at the fringes of inflammatory infiltrates.

Finally, the activity of MMPs in lung homogenates of WT and IRF-1-KO mice was analysed with an ELISA technique, in which substrate 1 is used to determine the joint activities of MMP-1, -2, -7, -8, -9, -12, -13, -14, -15, and substrate 2 is specifically cleaved by MMP-3 and -10 (Fig. 6A and B, respectively). In WT mice, which develop granuloma necrosis, MMP activity was increased relative to uninfected mice, at 20 weeks after infection. In IRF-1-KO mice, which do not develop granuloma necrosis, MMP expression was significantly lower at 20 weeks after infection.

In summary, these data corroborate the microarray-based hypothesis that IRF-1 driven granuloma necrosis may be associated with active proteolysis and matrix remodelling.

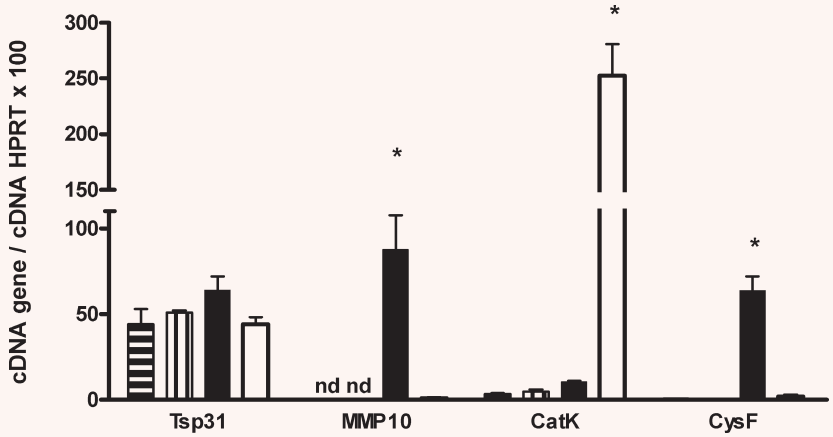

Fig. 4 Differential expression of proteolytic enzyme mRNAs in the lungs of infected mice. C57BL/6 WT (black bars) and IRF-1-deficient (white bars) mice were infected by aerosol with *M. avium* (TMC724, 10^5 CFU/mouse). Total RNA was prepared from the right lungs harvested 14 weeks after infection (filled black and white bars) as well as from the right lungs of uninfected mice (horizontally or vertically striped bars). One-microgram samples of total RNA from WT and KO mice were reverse transcribed to cDNA and amplified on a Light Cycler in parallel with a standard to calculate arbitrary units of expression. Gene expression levels for matrix metalloprotease 10 (MMP-10), cathepsin K (CatK) and cystatin F (CysF) were normalized to HPRT levels and the ratio was multiplied by 100. Tetraspanin 31 (Tsp31) was used as an unregulated control in IRF-1-KO compared to WT mice. $*P < 0.01$.

Table 2 Enrichment for gene ontology (GO) terms in IRF-1-dependent gene clusters

	Term	GO Ids	*P*-value	Count	Examples
Cluster B	Defence response	GO:0006952	1.24E-18	37	Ifnγ, Mx1, Gbp1, Indo, Nos2, Tnf, Wars
	Inflammatory response	GO:0006954	2.79E-13	23	Ccl1/2/7/19, Cxcl1/5/10/11/13, Il1a
	Antigen presentation	GO:0019882	6.26E-13	14	C2ta, CD1d, H2-Ab1, H2-DMa, H2-M3, Tap2, Tap2bp
	Antigen processing	GO:0019885	3.08E-06	4	
	T-cell activation	GO:0050870	5.42E-05	6	Cd4, Cd5, Cd86, H2-Oa, Il12a, Il2rg, Tnfsf13b
	B-cell mediated immunity	GO:0019724	1.77E-06	9	
	Isotype switching	GO:0048304	1.02E-04	3	Tbx21, Fcgr1, Cd40, Ifnγ, IgK-V1
	B-cell activation	GO:0050871	2.78E-06	6	
	Cell death	GO:0008219	1.64E-05	25	FasL, Cflar, Cdkn1a, Casp7, Dnase1l3, Hif1a, Lta, Tnf
	Apoptosis	GO:0006915	1.90E-05	24	
Cluster E	Chitin catabolism	GO:0006032	1.35E-06	3	Chi3l1, Chi3l3

Based on Fig. 3, groups of IRF-1-dependent M. avium-induced genes (cluster B) and genes overexpressed in IRF-1-deficient *M. avium*-infected lungs (cluster E) were analysed for enrichment of GO biological process annotation terms using the Bioconductor GO Stat algorithm [17]. Shown are selected highly significant GO terms and identifiers, including handpicked prototypic example genes.

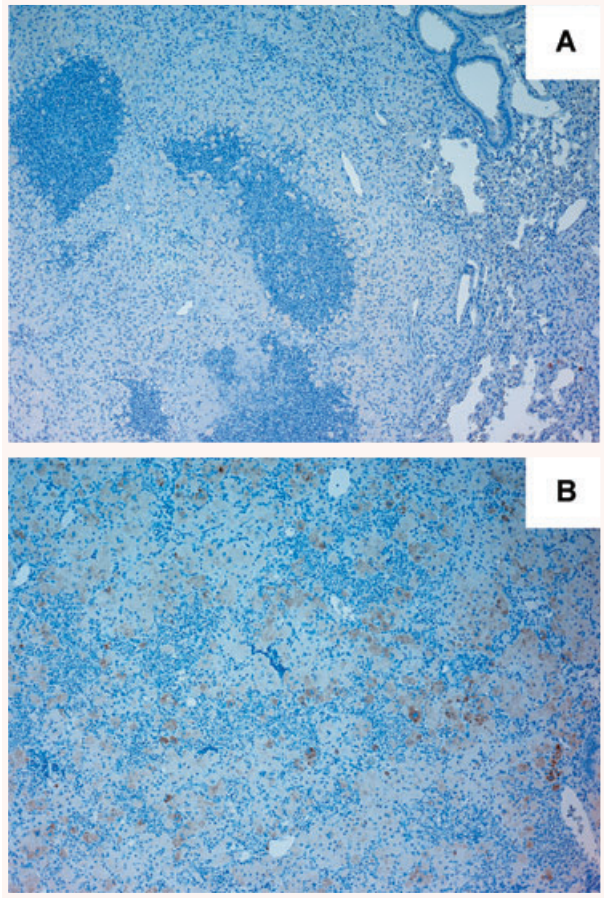

Fig. 5 Histopathology of infected mouse lungs. C57BL/6 (**A**) and IRF-1-KO (**B**) mice were infected by aerosol with *M. avium* (TMC724, 10^5 CFU/mouse). Twenty weeks after infection *M. avium*-infected mice were killed and the lung was removed. Lung sections were stained with an anti-cathepsin K antibody (original magnification ×20) and developed by the immunoperoxidase technique. Micrographs are representative of four mice examined.

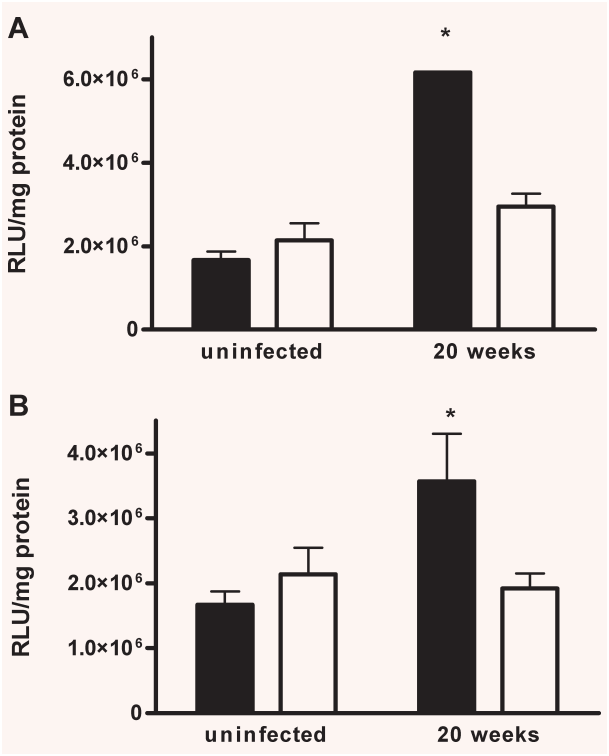

Fig. 6 Determination of MMP activity in lung homogenates of infected mice. C57BL/6 (black bars) and IRF-1-KO (white bars) mice were infected by aerosol with *M. avium* (TMC724, 10^5 CFU/mouse). Aliquots of lung homogenates were centrifuged at 300 × *g* for 10 min. Equal amounts of the supernatants were incubated with the fluorogenic MMP peptide substrate Mca-PLGL-Dpa-AR-NH2 (**A**: Combined activity of MMP-1, -2, -7, -8, -9, -12, -13, -14, -15) and Mca-RPKPVE-Nval-WRK (Dnp)-NH2 (**B**: combined activity of MMP-3 and MMP-10) at RT for 30 min. and subsequently analysed using a fluorescence microplate reader. The measured relative light units (RLU) were correlated to protein content in the lung homogenate and depicted as MMP activity [RLU/mg protein]).

Comparative evaluation of gene expression in the lungs of infected WT, IFN-γ-KO and IRF-1-KO mice reveals IRF-1 to be a critical inducer of type I immune responses

In a previous study, we investigated pulmonary gene expression in *M. avium*-infected IFN-γ-KO mice [6]. Because IRF-1 appears to mediate IFN-γ-induced granuloma necrosis but may be less critical for *M. avium* growth containment and overall survival, we analysed the data from both experiments together in order (*i*) to identify common target genes critical for granuloma necrosis and (*ii*) to determine the extent to which IFN-γ-induced pulmonary responses are IRF-1 dependent. By stringent statistical and fold-change filtering criteria a group of 2278 probe sets were identified and subjected to a *k*-means clustering algorithm that sorted all genes into eight clusters. Focussing on genes that are up-regulated during infection, four clusters with distinct patterns of gene expression were identified (Fig. 7, which includes associated GO terms and example genes, and Table S2 for lists of genes in different clusters). Cluster 1 consists of genes whose up-regulation depends on both IFN-γ and IRF-1, with enrichment in 'antigen presentation' (*H2* genes, *Cd1d*, *C2ta*, *Tap*) and 'lymphocyte activation'. In agreement with the shared absence of granuloma necrosis in both KO mouse strains, the GO term 'cell death' was also enriched in this cluster, suggesting that this cluster may contain critical effectors of granuloma necrosis. The second cluster contains IRF-1-dependent genes whose up-regulation is largely IFN-γ independent. In addition to genes controlling T-cell proliferation and phagocytosis, GO analysis identified enrichment for components

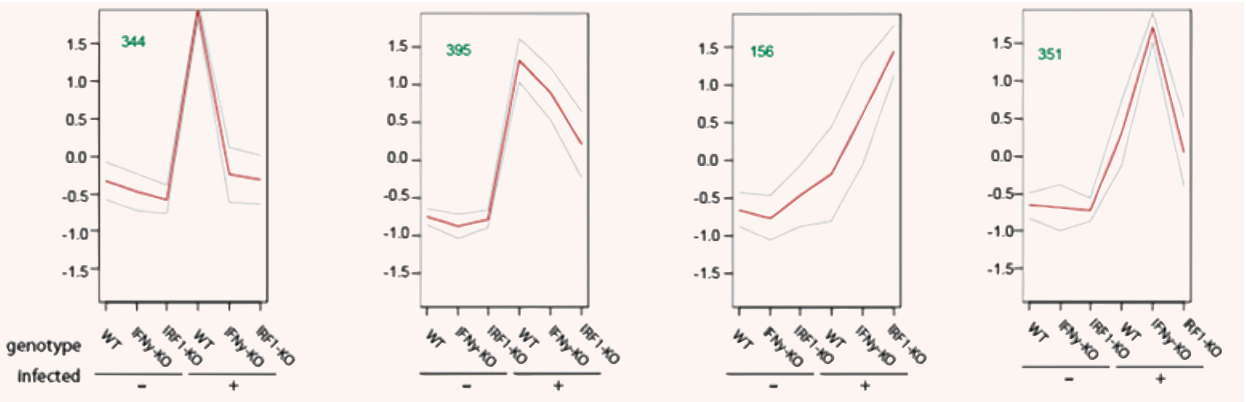

GO term	example	GO term	examples	GO term	example	GO term	example
antigen processing and presentation	Tap, Cd1d, B2m, H2, C2ta	Phagocytosis	Lcp2, Fcgr2b, Fcgr3, Fcer1g, Syk, Ndrg1	lipid biosynthesis	Idi1, Dhcr7, Dhcr24, Sc4mol, Cyp51	lysosome organization	Gba, Hexb, Cln3, Lyst
cell death	Casp7, Casp12, Tnfsf13b, Tnfrsf4, Ifi204	Glycolysis	Aldoc, Hk2, Pgk1, PFkl, Pkm2			osteoclast differentiation	Cd330lf, Inpp5d, Csf1, Tnf

Fig. 7 Comparative transcriptome analysis of *M. avium*-infected IRF-1- and IFN-γ-deficient mouse lungs. C57BL/6, IRF-1-KO and IFN-γ-KO mice were infected by aerosol with *M. avium* (TMC724, 10^5 CFU/mouse) in two separate experiments, each with its WT control. Cel files from both experiments were normalized together using RMA. Regulated genes were identified by a combination of statistical testing (limma F-test $P < 0.0001$) and absolute and relative changes in expression across all conditions (max-min > 80, max/min > 3). The resulting 2278 probe sets were *z*-score normalized and used for a *k*-means cluster analysis. Shown are the four clusters containing genes that are up-regulated in WT lungs after infection. Characteristic, significantly enriched GO biological process terms together with example genes are depicted below each cluster. Cluster 1 (top left): gene expression dependent on both IRF-1 and IFN-γ. Cluster 2 (top right): gene expression dependent on IRF-1 but less on IFN-γ. Cluster 3 (bottom left): overshooting gene expression mostly dependent on IRF-1. Cluster 4 (bottom right): overshooting expression mostly dependent on IFN-γ. Table S2 lists all probe sets and average expression data for clusters 1 to 4.

of the glycolytic pathway such as *Pgk1*, *Aldoc* and *Hk2.* Finally, deficiency in *Irf1* or *Ifn*γ also led to overshooting *M. avium*-induced gene expression (clusters 3 and 4). Interestingly, in the absence of *Irf1*, genes related to lipid metabolism were increased, whereas in *Ifng*-deficient lungs gene expression related to granulocyte and osteoclast differentiation and lysosome organization was enhanced. From each cluster two to three genes were selected for validation of the pattern of gene regulation by qRT-PCR (Fig. 8), essentially confirming the microarray data.

A schematic depiction of expression dynamics of the genes involved in the induction, signalling and effector functions of IFN-γ is shown in Fig. 9 (for signal intensities of individual genes see Table S3). It is evident that during *M. avium* infection most players are subject to regulation; strikingly, *Irf1* not only controls expression of IFN-γ-induced effector molecules like *Nos2* or *Irgm*, but also of signalling components (*Stat1/2*) and of *Ifn*γ itself. *In silico* analysis of transcription-factor-binding sites in the promoters of IFN-γ- and IRF-1-dependent *M. avium*-induced genes identified a shared enrichment of IRF-1 binding sites and ISRE sequences in both groups of genes (data not shown). The effect on IFN-γ expression levels may be indirect *via* a lack of recruitment or differentiation of T cells, because *Tcra* and *Il12rb1* mRNA levels are reduced in IRF-1 KO mice. Taken together, these data strongly suggest that IRF-1 not only is a key transcription factor downstream of IFN-γ, but may in fact be required for certain IFN-γ-independent transcriptional responses during mycobacterial infection of the lung.

Discussion

We used a robust *in vivo* model of mycobacteria-induced immunopathology to delineate mechanisms involved in granuloma necrosis [4, 6]. The signalling axis IFN-γ receptor/STAT-1/IRF-1 was identified as the critical pathway involved in the necrotizing process, whereas the IFN-αβ receptor and the IFN-γ-inducing cytokine IL-18 were not essential for granuloma necrosis. Furthermore, rigorous data mining of microarray-based gene expression analyses in WT and KO mice resulted in the identification of a subset of genes, induced by IFN-γ and IRF-1, which was associated with necrotizing immunopathology.

Since the times of Robert Koch, the differential manipulation of tissue damaging *versus* antibacterially protective events,

Fig. 8 Validation of cluster assignment for dependence on IFN-γ or IRF-1 by qRT-PCR. Lung RNA harvested from controls (mock) and 14 week infected WT/IFN-$\gamma^{+/+}$ (light grey), IFN-γ-KO (orange), WT/IRF-$1^{+/+}$ (dark grey) or IRF-1-KO (olive) mice was analysed for changes in expression of selected genes from clusters 1–4 according to Fig. 7. Expression was normalized to HPRT levels, using the WT/IRF-$1^{+/+}$ uninfected condition as a calibrator (fold change, FC = 1). Shown are mean + S.D. from six data points (three RNAs from individual mice, with 2 PCR replicates each).

simultaneously induced by the antimycobacterial immune response, has remained an attractive goal to complement the armamentarium of anti-TB therapy. However, only rabbits infected with *M. tuberculosis* develop characteristic cavities; guinea pigs suffering from TB exhibit severe central necrosis of pulmonary and lymph node granulomas that do not progress to full cavities [20, 21]. The mouse as a highly suitable, genetically and immunologically tractable model of TB pathogenesis [3] does not generally develop granuloma necrosis unless it is severely compromised, necrotic lesions then likely being the result of exacerbated mycobacterial growth early during infection. In order to take advantage of mouse strains genetically engineered to lack single components of the immune response for the analysis of mycobacteria-induced immunopathology, we developed a model that makes use of an aerosol challenge with the highly virulent strain of *M. avium* TMC724 [5]. In this model, the cells and mediators best known to be involved in mycobacterial growth retardation, $CD4^+$ T cells and IFN-γ, are also critically responsible for the necrotizing immunopathology [3, 4]. In contrast to *M. tuberculosis* infection, the high bacterial load present in the lung of *M. avium*-infected mice does not correlate with the extent of granuloma necrosis, thereby facilitating the evaluation of immunopathology as a feature largely independent of bacterial multiplication. Indeed, STAT-1-KO and IRF-1-KO had higher levels of *M. avium* in their lungs than WT mice, but did not develop granuloma necrosis. This is an important distinguishing characteristic of this model system, as mice deficient in STAT-1 or IRF-1 infected with *M. tuberculosis* were previously reported to exhibit extensive tissue necrosis due to excessive mycobacterial replication [22, 23], precluding any meaningful analysis of causative mediators of granuloma pathology in that model.

By disruption of key elements in the IFN-γ signalling pathway, we identified IRF-1 as the critical transcription factor associated with granuloma necrosis. Among the transcriptional patterns associated with the absence of granuloma necrosis in IRF-1-KO mice (Table 2 and Table S1), we found several tissue-remodelling genes such as cathepsins and matrix metalloproteases. Cathepsin K is a lysosomal cysteine endopeptidase that is widely expressed in bronchial epithelial cells, activated fibroblasts and also in infiltrating macrophages [24]. When specimens obtained from patients suffering from sarcoidosis, TB, granulomas caused by foreign materials and sarcoid-like lesions were investigated for the expression of cathepsin K, immunohistochemistry and *in situ* hybridization showed cathepsin K in epithelioid cells and multinucleated giant cells irrespective of the pathological condition and anatomical location, but not in normal resident macrophages [25]. Using cathepsin-K KO mice, increased lung fibrosis was observed after bleomycin challenge [26]. Thus, cathepsin K may be also involved in matrix degradation and may counteract the increased matrix deposition responsible for the development of lung fibrosis.

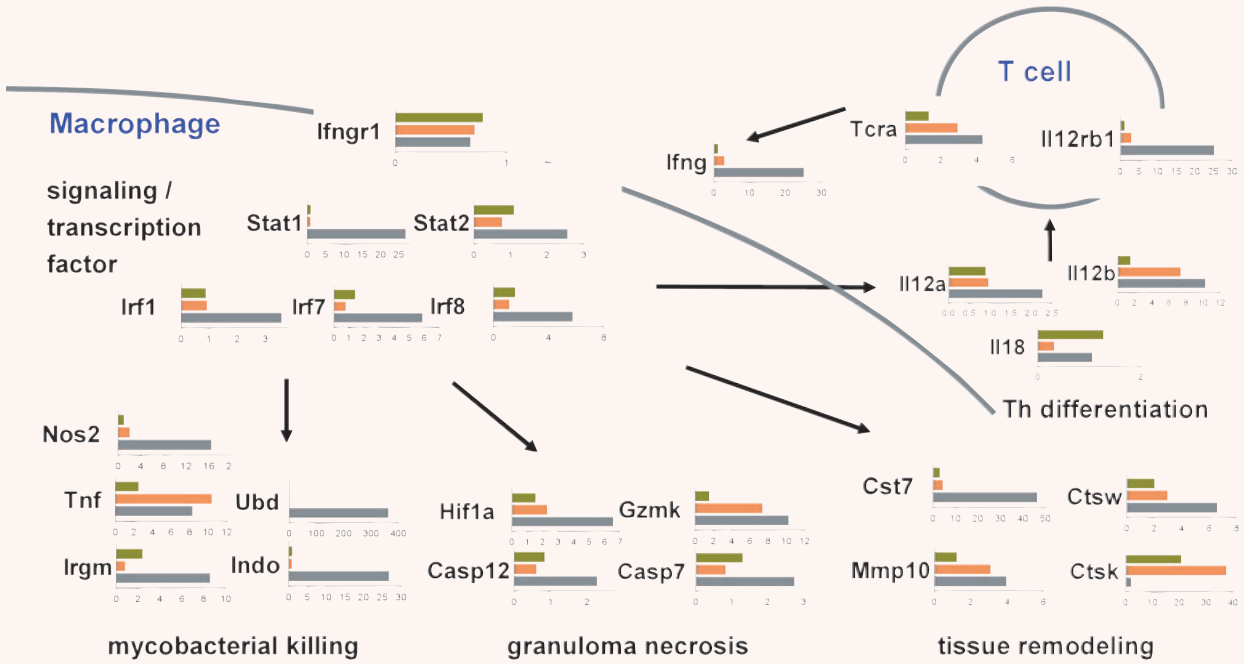

Fig. 9 Schematic representation of the type I immune response in *M. avium* infection and its transcriptional perturbation in *Irf1*- and *Ifn*γ-deficient mice. The pathway components of IFN-γ induction, signalling and effector functions are shown and assigned to macrophages and T cells as the prime host and effector cells during mycobacterial lung infection. The assignment of genes to the different effector function groups is tentative. Regulation of gene expression during *M. avium* infection in WT and gene-deficient mice is depicted as fold change relative to the respective uninfected control in bar plots (WT: grey bars; IRF-1-KO: olive bars; IFN-γ-KO: orange bars). The corresponding values are listed in Table S3.

Cystatin F is a known inhibitor of cathepsin K; reciprocal regulation of the two genes therefore suggests a co-ordinated matrix degradation program in IRF-1-KO mice infected with *M. avium* whose induction is substantially lower in WT mice. Additional membrane-degrading enzymes may also play a role, such as phospholipase A1 (PLA_1), which was regulated approximately 15-fold higher in WT compared to IRF-1-KO mice. PLA_1 hydrolyses fatty acids from phospholipids and produces lysophospholipids that have been implicated in various inflammatory processes [27]. Similarly, sphingomyelin phoshodiesterase, regulated ninefold higher in WT than in IRF-1-KO mice, is likely involved in ceramide turnover and regulated cell death [28].

Matrix metalloproteinases constitute a large family of Zn^{2+}- and Ca^{2+}-dependent endopeptidases that have been implicated in chronic inflammatory responses and tissue remodelling (reviewed in [29]). *M. tuberculosis* was previously demonstrated to elicit the expression of MMP-2 and MMP-9 [30]. Non-specific blocking of MMPs in C57BL/6 mice early during infection with *M. tuberculosis* reduced bacterial dissemination *via* the bloodstream, suggesting that MMPs play a role in facilitating dissemination, likely *via* extracellular matrix degradation [31]. Mice treated with a non-specific blocker of MMPs also had increased collagen deposition within early granulomas and significantly decreased pulmonary leucocyte recruitment when compared to vehicle-treated, *M. tuberculosis*-infected mice [32]. Another study showed that MMP-9, specifically, is required for recruitment of macrophages and tissue remodelling to allow for the formation of tight, well-organized granulomas [31]. Little is known about any specific involvement of the stromelysin MMP-10 in chronic granulomatous diseases, such as TB. It is possible that strong IRF-1-mediated up-regulation of MMP-10 was detected in our experiments because MMP-10 induction is more apparent in infections with *M. avium* than with *M. tuberculosis*. Clearly, the overall fine-tuning and specificity of, on the one hand, lysosomal protease down-regulation and, on the other hand, simultaneous matrix metalloproteinase up-regulation, that appears to correlate with granuloma necrosis in our model, needs further comparative exploration in selectively transgenic mouse strains.

Our initial rationale to analyse gene expression in IRF-1-KO lungs was based on the essential role of IRF-1 as a downstream transcription factor required for directing the expression of many (but probably not all) IFN-γ-dependent genes. Because the biological effects of IFN-γ were only partially dependent on IRF-1 (granuloma necrosis *yes*, survival *no*), we reasoned that the identification of a smaller group of genes whose induction was abrogated both in IFN-γ-KO and IRF-1KO mice would narrow down the set of candidate mediators of granuloma necrosis. Our expectation that

IRF-1 would be required only for a subset of IFN-γ-dependent genes was, however, challenged by the experimental results that revealed a more important and reciprocal role for IRF-1 than anticipated. In addition to obvious IFN-γ target genes (such as NOS2, Mx1, Gbp1, etc.) IRF-1 was also essential for the induction of many genes involved in the induction of IFN-γ expression (particularly, *Il12b*, *Il12rb1*, *Ifnγ* itself) as well as of some components of the IFN-γ signalling machinery (*Ifngr*, *Stat1*). Thus, the unexpectedly large size of cluster 2 in our comparative analysis of the IRF-1- and IFN-γ-induced transcriptome indicates that IRF-1 plays a role in additional pathways and is activated by stimuli other than IFN-γ. Of note, within the constraints and sensitivity limits of the cluster algorithm used, no cluster consisting of IFN-γ dependent, but IRF-1-independent genes was observed, suggesting that IRF-1 is indeed required for most IFN-γ-dependent transcriptional responses in the lung.

In retrospect, this broader role for IRF-1, evident from our microarray analysis in a complex *in vivo* model system, is consistent with the function very recently ascribed to IRF-1 in the response of DC to TLR stimulation *in vitro* and in T helper cell differentiation to a Th1 phenotype in general [33, 34]. Kano *et al.* demonstrate that IRF-1, by directly interacting with and activating the Il12rb1 promoter in $CD4^+$ T cells, controls the development of Th1 cells independently of and in addition to the transcription factor T-bet [34]. Given that $CD4^+$ cells, IL-12 and IFN-γ are all necessary for the initiation of granuloma necrosis, IRF-1 may therefore primarily serve as an upstream regulator of Th1 differentiation also in our model of mycobacteria-induced immunopathology. Alternatively or additionally, IRF-1 may govern central necrotization of mycobacteria-induced granulomas by regulating downstream tissue-damaging pathways.

Among the genes transcriptionally regulated in both IRF-1-KO and IFN-γ-KO mice (Fig. 7, Table S2), there are some interesting candidates for further functional evaluation. As previously noted, the up-regulation of chemokines with angiostatic properties, such as CXCL10 and CXCL11 is completely abrogated in both KO mouse strains. It has previously been argued that hypoxia, due to reduced neo-angiogenesis within the growing granuloma, contributes to granuloma necrotization [6]. One of the most prominently up-regulated genes (approximately 200–300-fold in WT *versus* IRF-1-KO and IFN-γ-KO mice) was *ubiquitin D*. Specific peptide sequences within ubiquitin D were recently shown to have antimycobacterial activity and were implicated in a putative, lysosomal killing pathway for mycobacteria [35]. The role of ubiquitin D in the immunopathogenesis of TB is unknown, although it might be argued that enhanced targeting of proteins for degradation may be an intracellular correlate of tissue destruction. Another prominently regulated gene was *nos2* (nitric oxide synthase 2). NOS2 clearly regulates antimycobacterially effective macrophage responses [36], although conspicuously not during *M. avium* infection in mice [37], which may explain why IRF-1-KO mice (like NOS2-KO mice) do not succumb to infection earlier than WT mice. However, we and others previously demonstrated that NOS2 is not involved in granuloma necrosis in this mouse model of mycobacteria-induced immunopathology [4, 38]. It would therefore seem that not all, but only a limited number of genes transcriptionally controlled by IRF-1 are critical for granuloma necrosis. Quite possibly, these are members of the GO cluster 'cell death and apoptosis' whose transcriptional response was dependent on IRF-1 and IFN-γ (Figs. 7 and 8).

In conclusion, this study demonstrates that *ex vivo* microarray profiling of lungs obtained from mice with different pathological responses to *M. avium* infection yields novel candidate genes that may be causally involved in granuloma necrosis and that may now be further validated with suitable depletion or neutralization strategies.

Supporting Information

Tables S1: Genes regulated more than fivefold in the lungs of WT *versus* IRF-1-KO mice infected with *M. avium*.

WT and IRF-1-KO mice were infected by aerosol with *M. avium* (TMC724, 10^5 CFU/mouse) and gene expression was analysed in RNA extracted from the lungs at 14 weeks after infection by the Affymetrix Mouse 430A_2 GeneChip, containing a total of 22,690 probe sets. The fold change (FC) is the ratio of average gene expression values in infected compared to uninfected mice (C). Shown are only those genes with a more than fivefold difference in gene expression between infected WT and infected IRF-1-KO mice. The assigned cluster is indicated according to Fig. 5: all genes up-regulated more than fivefold in WT, are assigned to cluster B, whereas all genes up-regulated more than fivefold in IRF-1-KO, except Gzma, are assigned to clusters D, E and F. Repetitive probe sets have different target sequences and might represent alternative splice variants of the same expressed gene. Two-way ANOVA q-value <0.01 in all cases.

Table S2: IFN-γ- and IRF-1-dependent gene expression according to *k*-means clusters shown in Fig. 7

For all probe sets sorted by the *k*-means clustering into clusters 1–4 depicted in Fig. 7, the probe set ID, gene symbols, gene description, average expression values for all conditions and fold changes of infected compared to mock treated controls, is shown. Data for the different clusters are shown in separate sheets.

Table S3: Regulation of IFN-γ-pathway genes in *M. avium* infection which are dependent on IFN-γ and IRF-1 (as depicted in Fig. 9)

For all genes whose regulation is depicted in Fig. 9, the fold changes of infected *versus* mock controls, as well as the average expression values for each condition, are shown.
This material is available as part of the online article

Acknowledgements

We are grateful to A. Servatius, H. Dietrich and S. Kröger for expert technical assistance, and to A. Malzan and I. Monath for experimental logistics and mouse breeding. We thank O. Liesenfeld of the Free University of Berlin, for providing IL-18-KO mice. This work was supported in part by a DFG grant to S.E. (SFB367-C9), by BMBF grants to S.E. (NIE-S05T22, 01KI0784F) and to R.L. (FKZ 01GS0402). The authors have no conflicting financial interests.

References

1. **Ehlers S, Hölscher C.** DTH-associated pathology. In: Kaufmann SH, Steward MW, editors. Topley & Wilson's microbiology and microbial infections: immunology. London: Hodder Arnold; 2005. pp. 705–29.
2. **Dheda K, Booth H, Huggett JF, *et al.*** Lung remodeling in pulmonary tuberculosis. *J Infect Dis.* 2005; 192: 1201–9.
3. **North RJ, Jung YJ.** Immunity to tuberculosis. *Annu Rev Immunol.* 2004; 22: 599–623.
4. **Ehlers S, Benini J, Held HD, *et al.*** Alphabeta T cell receptor-positive cells and interferon-gamma, but not inducible nitric oxide synthase, are critical for granuloma necrosis in a mouse model of mycobacteria-induced pulmonary immunopathology. *J Exp Med.* 2001; 194: 1847–59.
5. **Benini J, Ehlers EM, Ehlers S**. Different types of pulmonary granuloma necrosis in immunocompetent vs. TNFRp55-gene-deficient mice aerogenically infected with highly virulent Mycobacterium avium. *J Pathol.* 1999; 189: 127–37.
6. **Aly S, Laskay T, Mages J, *et al.*** Interferon-gamma-dependent mechanisms of mycobacteria-induced pulmonary immunopathology: the role of angiostasis and CXCR3-targeted chemokines for granuloma necrosis. *J Pathol.* 2007; 212: 295–305.
7. **Rhoades ER, Frank AA, Orme IM.** Progression of chronic pulmonary tuberculosis in mice aerogenically infected with virulent Mycobacterium tuberculosis. *Tuber Lung Dis.* 1997; 78: 57–66.
8. **Holscher C, Holscher A, Ruckerl D, *et al.*** The IL-27 receptor chain WSX-1 differentially regulates antibacterial immunity and survival during experimental tuberculosis. *J Immunol.* 2005; 174: 3534–44.
9. **Chomczynski P, Mackey K.** Substitution of chloroform by bromo-chloropropane in the single-step method of RNA isolation. *Anal Biochem.* 1995; 225: 163–4.
10. **Chomczynski P, Sacchi N.** Single-step method of RNA isolation by acid guanidinium thiocyanate-phenol-chloroform extraction. *Anal Biochem.* 1987; 162: 156–9.
11. **Benjamini Y, Hochberg Y.** Controlling the false discovery rate: a practical and powerful approach to multiple testing. *J R Stat Soc B.* 1995; 57: 289–300.
12. **Sturn A, Quackenbush J, Trajanoski Z.** Genesis: cluster analysis of microarray data. *Bioinformatics.* 2002; 18: 207–8.
13. **Bolstad BM, Irizarry RA, Astrand M, *et al.*** A comparison of normalization methods for high density oligonucleotide array data based on variance and bias. *Bioinformatics.* 2003; 19: 185–93.
14. **Knight CG, Willenbrock F, Murphy G.** A novel coumarin-labelled peptide for sensitive continuous assays of the matrix metalloproteinases. *FEBS Lett.* 1992; 296: 263–6.
15. **Nagase H, Fields CG, Fields GB.** Design and characterization of a fluorogenic substrate selectively hydrolyzed by stromelysin 1 (matrix metalloproteinase-3). *J Biol Chem.* 1994; 269: 20952–7.
16. **Flynn JL, Chan J.** Immunology of tuberculosis. *Annu Rev Immunol.* 2001; 19: 93–129.
17. **Losana G, Rigamonti L, Borghi I, *et al.*** Requirement for both IL-12 and IFN-gamma signaling pathways in optimal IFN-gamma production by human T cells. *Eur J Immunol.* 2002; 32: 693–700.
18. **Aly S, Wagner K, Keller C, *et al.*** Oxygen status of lung granulomas in Mycobacterium tuberculosis-infected mice. *J Pathol.* 2006; 210: 298–305.
19. **Gentleman RC, Carey VJ, Bates DM, *et al.*** Bioconductor: open software development for computational biology and bioinformatics. *Genome Biol.* 2004; 5: R80.
20. **Basaraba RJ, Dailey DD, McFarland CT, *et al.*** Lymphadenitis as a major element of disease in the guinea pig model of tuberculosis. *Tuberculosis (Edinb.).* 2006; 86: 386–94.
21. **Converse PJ, Dannenberg AM Jr, Estep JE, *et al.*** Cavitary tuberculosis produced in rabbits by aerosolized virulent tubercle bacilli. *Infect Immun.* 1996; 64: 4776–87.
22. **Sugawara I, Yamada H, Mizuno S.** STAT1 knockout mice are highly susceptible to pulmonary mycobacterial infection. *Tohoku J Exp Med.* 2004; 202: 41–50.
23. **Yamada H, Mizuno S, Sugawara I.** Interferon regulatory factor 1 in mycobacterial infection. *Microbiol Immunol.* 2002; 46: 751–60.
24. **Buhling F, Waldburg N, Reisenauer A, *et al.*** Lysosomal cysteine proteases in the lung: role in protein processing and immunoregulation. *Eur Respir J.* 2004; 23: 620–8.
25. **Buhling F, Reisenauer A, Gerber A, *et al.*** Cathepsin K – a marker of macrophage differentiation? *J Pathol.* 2001; 195: 375–82.
26. **Buhling F, Rocken C, Brasch F, *et al.*** Pivotal role of cathepsin K in lung fibrosis. *Am J Pathol.* 2004; 164: 2203–16.
27. **Aoki J, Nagai Y, Hosono H, *et al.*** Structure and function of phosphatidylserine-specific phospholipase A1. *Biochim Biophys Acta.* 2002; 1582: 26–32.
28. **Tani M, Ito M, Igarashi Y.** Ceramide/sphingosine/sphingosine 1-phosphate metabolism on the cell surface and in the extracellular space. *Cell Signal.* 2007; 19: 229–37.
29. **Parks WC, Wilson CL, Lopez-Boado YS.** Matrix metalloproteinases as modulators of inflammation and innate immunity. *Nat Rev Immunol.* 2004; 4: 617–29.
30. **Quiding-Jarbrink M, Smith DA, Bancroft GJ.** Production of matrix metalloproteinases in response to mycobacterial infection. *Infect Immun.* 2001; 69: 5661–70.
31. **Taylor JL, Hattle JM, Dreitz SA, *et al.*** Role for matrix metalloproteinase 9 in granuloma formation during pulmonary Mycobacterium tuberculosis infection. *Infect Immun.* 2006; 74: 6135–44.
32. **Izzo AA, Izzo LS, Kasimos J, *et al.*** A matrix metalloproteinase inhibitor promotes granuloma formation during the early phase of Mycobacterium tuberculosis pulmonary infection. *Tuberculosis (Edinb.).* 2004; 84: 387–96.
33. **Schmitz F, Heit A, Guggemoos S, *et al.*** Interferon-regulatory-factor 1 controls

Toll-like receptor 9-mediated IFN-beta production in myeloid dendritic cells. *Eur J Immunol.* 2007; 37: 315–27.

34. **Kano S, Sato K, Morishita Y, *et al.*** The contribution of transcription factor IRF1 to the interferon-gamma-interleukin 12 signaling axis and T(H)1 *versus* T(H)-17 differentiation of CD4(+) T cells. *Nat Immunol.* 2008; 9: 34–41.
35. **Alonso S, Pethe K, Russell DG, *et al.*** Lysosomal killing of Mycobacterium mediated by ubiquitin-derived peptides is enhanced by autophagy. *Proc Natl Acad Sci USA.* 2007; 104: 6031–6.
36. **MacMicking JD, North RJ, LaCourse R, *et al.*** Identification of nitric oxide synthase as a protective locus against tuberculosis. *Proc Natl Acad Sci USA.* 1997; 94: 5243–8.
37. **Gomes MS, Florido M, Pais TF, *et al.*** Improved clearance of Mycobacterium avium upon disruption of the inducible nitric oxide synthase gene. *J Immunol.* 1999; 162: 6734–9.
38. **Florido M, Cooper AM, Appelberg R.** Immunological basis of the development of necrotic lesions following Mycobacterium avium infection. *Immunology.* 2002; 106: 590–601.